Process Simulation for Molten Carbonate Fuel Cells[×]

M. Fermeglia[1,2]*, A. Cudicio[1], G. DeSimon[1], G. Longo[2], and S. Pricl[1]

[1] Computer-Aided Systems Laboratory, DICAMP, University of Trieste, Piazzale Europa 1, 34127 Trieste, Italy
[2] ICS-UNIDO, Area Science Park, Padriciano 99, 34100 Trieste, Italy

Received July 5, 2004; accepted August 24, 2004

Abstract

In the framework of electricity production from molten carbonate fuel cells (MCFC), this work presents the results obtained from steady state process simulation, coupled with a detailed dynamic model for the cell. The derivation of the model is briefly outlined, and detailed results of the simulation are reported. Macroscopic state variables of the overall system process are investigated by means of sensitivity analysis, yielding clear directions for process improvement and optimisation. The detailed steady state and dynamic simulation of the MCFC for a bi-dimensional cross flow configuration showed the importance of the state variable distribution in the cell. Both models were based on data from real plants, and the simulation conditions were selected according to real operating conditions. The process studied was a 500 kW MCFC power system based on Ansaldo fuel cell (AFC) technology. The steady state simulation revealed the main interactions among the different devices involved in the process, and the subsequent sensitivity analysis showed that there is room for improvement in electrical efficiency by increasing: i) the steam to methane ratio, ii) the pressure, and iii) the air feed ratio. The dynamic simulation yielded the quantitative response of the system to several, different, perturbations and proved to be a valid tool for determining temperature, current, and voltage profiles as a function of time, within the fuel cells.

Keywords: Chemical Reaction, Dynamic Modelling, Molten Carbonate Fuel Cells, Process Simulation

1 Introduction

Fuel-cell systems, which are virtually free from noxious emissions of nitrogen oxides normally associated with burning fossil fuels, are becoming more and more important after the deregulation of the electricity market. A fuel cell can convert chemical energy into electricity with great efficiency, thus conserving fuel resources and reducing CO_2 emissions. Hydrogen is considered an ideal fuel for many energy-conversion systems, but its use is strongly dependent on technological breakthroughs in cost and storage. Hence, it is reasonable to assume that, in the immediate future, hydrocarbons (e.g. methane) or alcohols (e.g. methanol) will constitute the main fuels for fuel cells. Using methane as the primary fuel favours devices that operate at high temperatures, such as molten carbonate and solid oxide fuel cells. These are able to electrochemically oxidize a mixture of hydrogen and carbon monoxide, which is generated internally from the natural gas within the fuel cell stack.

Among the different fuel cells developed so far, molten carbonate (MCFC) fuel cells, also referred to as "second generation" cells [1], have been extensively investigated in the last decade as they present several advantages with respect to other technologies. Thus, MCFC simulation may be helpful in their further development before commercialisation [2, 3]. In fuel cells and in the MCFC in particular, high overall efficiency with respect to other electrical energy production systems can be reached by virtue of many concurrent factors [4, 5]. Even though fuel cells have been intensively studied in recent years, some open problems still remain, such as corrosion and lifetime, which undoubtedly constitute the major drawbacks towards commercialisation.

A MCFC plant integrates a stack with a fuel conditioning pre-treatment, essentially consisting of desulphurisation and reforming, and post treatments of residual energy recovered by steam and gas micro-turbines. The stack is made up of a number of piled up cells, with heat exchange between the different cell components; thermal control is obtained by varying both the exhaust gas recycle and the inlet temperature.

[×] *Article is part of Topical Issue 'Modelling of Fuel Cell Systems'*

[*] *Corresponding author, Maurizio.Fermeglia@dicamp.units.it*

 DOI: 10.1002/fuce.200400049

Many related parameters concur to define the optimum process conditions, and its stability with respect to possible external perturbations. Thus, it is essential to simulate the entire process for different steady state conditions in order to determine the best process parameters, and to study the effect of process modifications with respect to efficiency and energy production. At the same time, the study of the dynamic behaviour of the process for determining the time dependence of key process parameters for system changes is also challenging and of paramount importance.

Mathematical modelling is used as an investigational technique to improve the knowledge of the limiting factors [6]. In the past few years, many authors have developed steady state models, based on macro balances [7], applied to both single cell and stack, or on differential equations [8–14], applied to both mean and distributed variables. An interesting review of the steady state simulation of fuel cells is reported in [15], in which it is stressed that most researchers used basically the same mass and heat balance equations for cells or stacks. Only a few authors performed calculations of flow fields from momentum balances [15, 16]. Overpotential and polarization effects have been treated in very different ways by different authors. Models for electrodes were developed assuming various structures for the micro-pores and internal meniscus [17–19], but such models are not always easily integrated in the macrostructure to be simulated. Many issues have been addressed and solved assuming various hypotheses, in the formulation of equations, and in the approximation of accessory devices [17], but many others still need to be solved, like the integration of the cell model in the plant and control strategies. To account for such issues, the dynamic simulation of the MCFC cell is necessary. So far, the approaches described in the literature were carried out assuming separated modules [20–24], exchanging information among them, and solving the system by means of a sequential modular approach. Each module is solved and the results are passed on to the next module until convergence is achieved. Specific modules are used to calculate electrical, physical, and chemical properties. Recently, another interesting approach [25] considered the dynamic simulation of a MCFC with internal reforming and one-dimensional counter flow with isobaric conditions in the duct. The model yielded interesting results for the simplified case of negligible heat conduction and lumped solid phases. The model was written in terms of dimensionless variables, and tested for the stepped input of some variables.

In this paper, some details of the simulation of a MCFC process under steady state condition are reported, together with the dynamic behaviour of a two-dimensional model for the single cell, which is an assembly of cathode, electrolyte, and anode with a cross flow configuration. The coupling of a process simulation model with a detailed (steady state and dynamic) model of the cell has important practical advantages for the investigation of the performance and industrialization of the system. The detailed simulation of the cell is useful for its optimisation, and also for adjusting the overall conditions of the system to the detailed behaviour of the cell. Useful information may be obtained from the detailed simulation of the cell: (i) temperature distribution, to understand

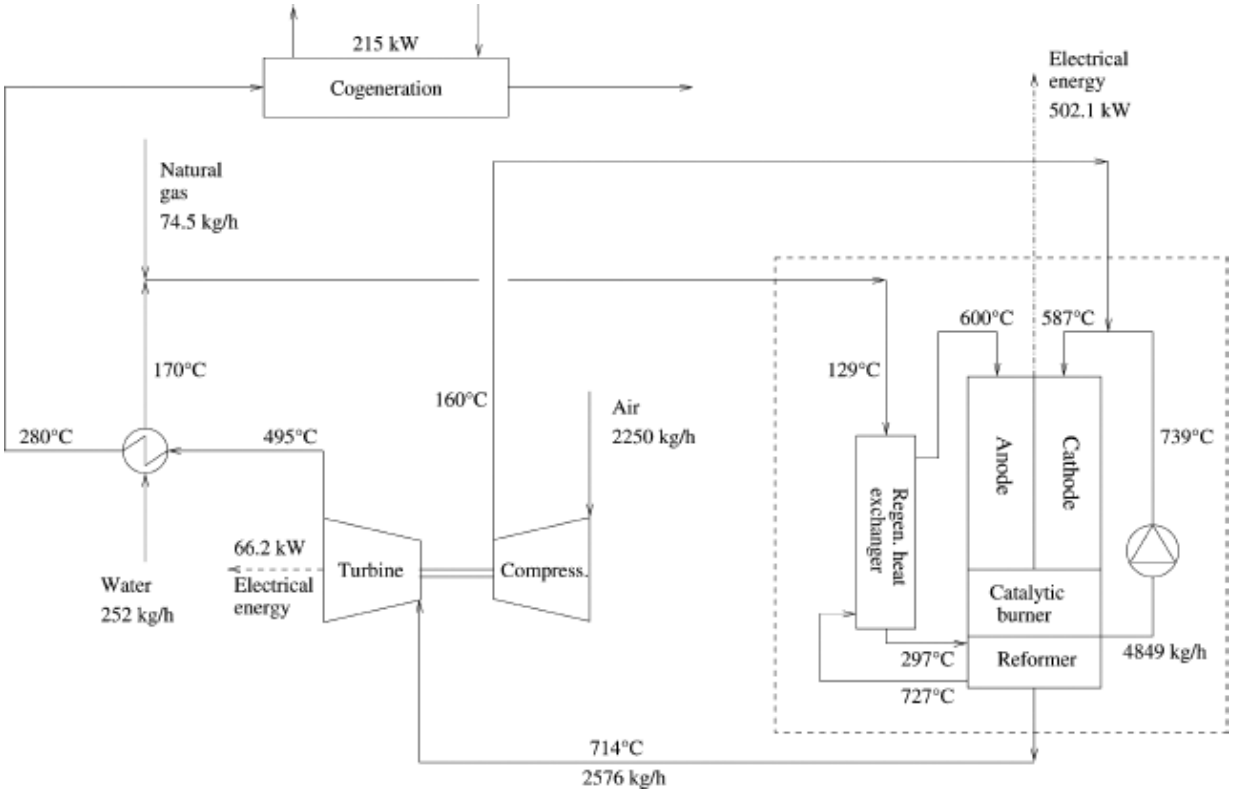

Fig. 1 General flow sheeting of a MCFC based electricity production process showing all the main elements and the numerical values for the base case.

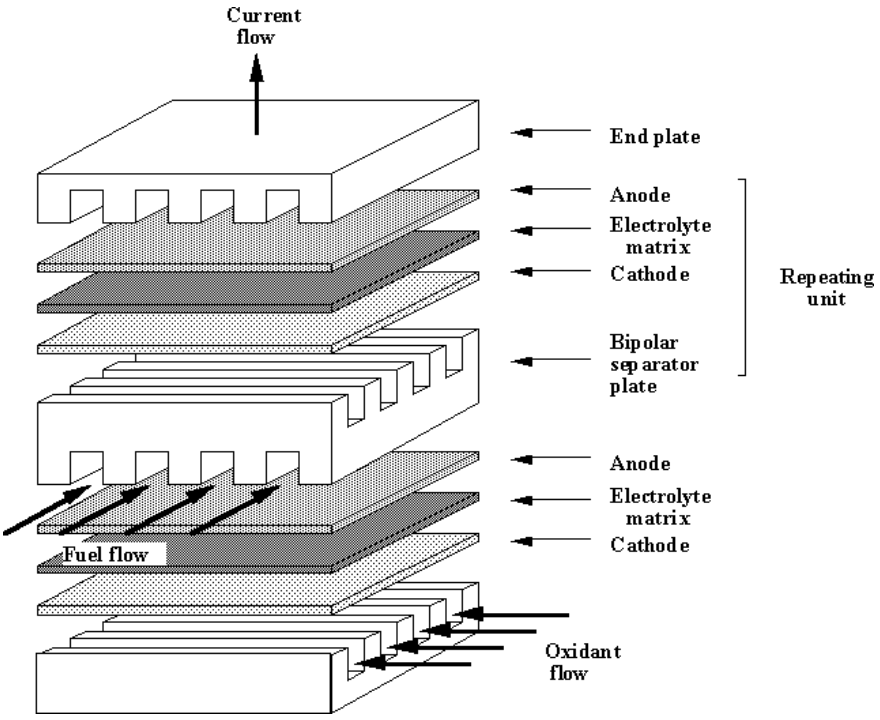

Fig. 2 Schematic diagram of a MCFC showing the different components.

non-homogeneity and temperature peaks; (ii) concentration profiles and molar flow rates, to highlight parts of the cell not functioning properly; and (iii) cell current density distribution. In order to obtain reasonable results, the process model and the detailed cell model must be consistent.

Figure 1 shows the general process for energy production. Figure 2 shows the essential geometry of the single cell, as modelled in this paper.

The steady state process simulation is carried out using the commercial software Aspen plus™ by Aspentech™. The process model is derived by assembling library modules for most of the unit operations involved, including turbines, reactors, compressors, and heat exchangers. Since the MCFC unit operation is not available in the software, a Fortran90 module has been developed and interfaced with the simulator. The modules developed both from the library and in-house make use of the physical and chemical property data and methods stored in the Aspen plus™ thermodynamic library. Details on the derivation of the model are reported in [26].

The dynamic simulation approach considered in this paper is based on a two dimensional representation of a cross flow MCFC (Figure 2), in which all the relevant internal variables are distributed along the surface considered in the simulation [27]. The model accounts for heat transfer by convection and conduction, and for each solid phase (anode, cathode, and electrolyte) the gaseous flux is considered separately, each with its own physical properties, characteristics, and model equations. Heat conduction in the electrode is considered to be negligible. The input variables are the velocities, temperatures, and densities, and the water gas shift reaction is considered to be instantaneous and constrained by the continuity equation (the principle of mass conservation for flowing systems). The model is written in terms of dimensional variables, and tested for a wide range of input variable variations: steps, linear ramps, and sinusoidal ramps. Equations are grouped together logically, but not analytically, in structured modules (duplicated variables are eliminated during the solution), thus allowing simple and fast modifications of the system for screening many different configurations. Chemical reactions are coupled with homogeneous and heterogeneous heat and mass transfer, thus generating a system of non-linear differential equations.

The dynamic model of the cell is consistent with the simplified steady state model used in the process simulation, thus providing a complete tool for the investigation of the main characteristics of the MCFC process in view of an industrial application.

In the next section a summary of the model development for the whole process is reported, followed by a detailed description of the single cell model. The detailed model equations are derived in transient conditions. Subsequently, the model implementation in the AES (Aspentech Engineering Suite™) process simulation software is illustrated separately for the steady state process model, carried out with Aspen plus™, and for the dynamic simulation of the cell, performed with Aspen Custom Modeler™. In both cases, the Aspen Property Plus™ package was used for the determination of all the thermophysical properties for the systems of interest.

2 Model Development

2.1 The Energy Production Process

The molten carbonate fuel cell plant described in the introduction, and reported in Figure 1, is the reference flow sheet for the development of the steady state simulation of the process. Figure 2 shows the essential geometry of the single cell as modelled in this paper. The main components of the MCFC are: (i) two metal current collectors, also active in distributing the gas streams across the electrodes surfaces; (ii) a NiO-based porous cathode, where the reduction reaction occurs, resulting in the production of the CO_3^2 ion, that must travel across (iii) an electrolyte tile (made up of molten K, Na, and Li carbonates in a solid porous and inert matrix), and reach (iv) a Ni-based porous anode, where oxidation occurs.

The cathode reaction is:

$$CO_{2,c} + \frac{1}{2}O_2 + 2^- \rightarrow CO_3^{2-} \quad (1)$$

The anode reaction is:

$$H_2 + CO_3^{2-} \rightarrow H_2O + CO_{2,a} + 2e^- \quad (2)$$

The overall reaction is essentially the hydrogen combustion reaction, combined with a CO_2 transfer from cathode to anode:

$$H_2 + \frac{1}{2}O_2 + CO_{2,c} \rightarrow H_2O + CO_{2,a} \quad (3)$$

The stack is made up of a number of piled up cells, separated by cooling plates, used to maintain a constant temperature, and soft joints, to comply with mechanical tolerances.

Natural gas, after a primary treatment, is mixed with steam, pre-heated in a regenerative heat exchanger, and fed to the reformer, where CO and H_2 are produced. Exit gas again passes through the regenerative exchanger, and is set ready to be processed at the anodic side of the fuel cell stack. After electrochemical and gas shift conversion, a residual concentration of fuel is still present, principally because CH_4 unconverted in the reformer is inert in the stack. Moreover, to avoid a diffusion-controlled electrochemical process, not all the H_2 and CO are consumed. Consequently, fuel containing effluent is mixed with part of the cathodic exhaust, and fed to a catalytic burner where the heat necessary for the endothermic reactions taking place in the reforming process is produced and directly exchanged. The CO_2, rich and hot, gas is mixed with fresh air coming from the compressor, and is fed to the cathode where O_2 and CO_2 are consumed by reaction Eq. (1). Part of the cathode exhaust gas is sent to a turbine for recovering residual energy, which is used to drive the air compressor and to produce further electrical energy. The hot effluent eventually releases the heat necessary to produce reforming steam, and for a possible cogeneration.

2.2 The MCFC Dynamic Model

The model development starts from the equations of change expressed in two dimensions. Details of the derivation of the model can be found in [27]. To describe the bi-dimensional distribution of variables in the cell it is necessary to consider all the electrochemical equations involved in the phenomena. These are: (i) the Nernst equation, (ii) the polarization effects, (iii) the Butler-Volmer equation, and (iv) the model of the electrodes. The first equation relates the open circuit voltage of the fuel cell with the standard voltage:

$$V_0 = E_0 + \frac{RT}{nF}\ln\frac{P_{H_2}P_{O_2}^{1/2}P_{CO_{2_C}}}{P_{H_2O}P_{CO_{2_A}}} \quad (4)$$

Even though authors distinguish between different polarization sources, in most cases they are reduced to a general polarization at the anode and cathode, and ohmic polarizations at the electrolyte. In this work, the same approach is used according to the following equation:

$$\eta = R_e + \eta_A + \eta_C \Rightarrow V = V_0 - \eta i \quad (5)$$

The relationship between cell current and cell voltage under load (Butler-Volmer equation) is as follows:

$$i = \vec{i} - \overleftarrow{i} = i_0\left(e^{\beta nF\eta i/RT} - e^{-(1-\beta)nF\eta i/RT}\right) \quad (6)$$

where η is the resistance (other symbols are explained in the list of symbols). A basic assumption enabling the application of Butler-Volmer kinetics to the complete cell (anode and cathode) is the quasi-equilibrium of the anodic reactions, and the negligible ion conduction resistance of the electrolyte. With these assumptions, the cathodic reaction is the rate determining process step, and Butler-Volmer kinetics are applied to describe the current density.

In Eq. (6) the exchange current density is a function of component partial pressures, through a so-called standard exchange current density coefficient, valid under the same assumptions reported above:

$$i_0 = i_0\left(i_0^0, P_{O_2}, P_{CO_{2_C}}, T\right) \quad (7)$$

In order to derive the working equations from the prime principles described above, some further assumptions have been made to simplify the model. Such assumptions are briefly summarized as follows (see Figure 3 for axis definition and model geometry): (i) the ideal gas law is assumed, and mixture effects on densities are ignored; (ii) the anode feed is composed of CH_4, CO, CO_2, H_2, and H_2O; (iii) the cathode feed is composed of CO_2, N_2, and O_2; (iv) the electrolyte is composed of K_2CO_3, Li_2CO_3, and Na_2CO_3; (v) the system is adiabatic; (vi) the reaction rate is a function of current; (vii) thick channel distribution on the cell plane, so ribs are neglected; (viii) perfect mixing and negligible diffusion flow in the direction of flow; (ix) nitrogen oxides at the cathode and ammonia at the anode are ignored; (x) a bi-dimensional model is assumed, and velocities and their derivatives along the z-axis neglected; (xi) equal current distribution at the electrodes; (xii) plug flow; (xiii) Nusselt number, which is used to compute the heat transfer coefficients in the equations of

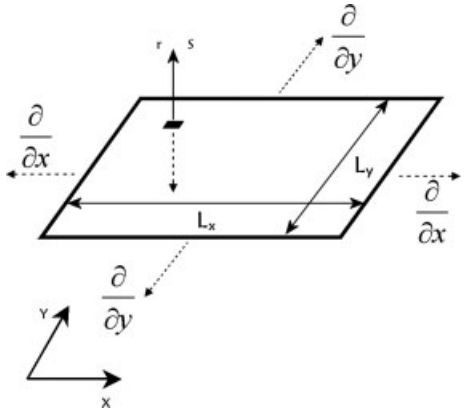

Fig. 3 Reference system for the development of the model equations, the flow direction is *y*.

change (Eqs. (8) and (11)), is function of Prandtl number, Reynolds number, and geometrical factor, and (xiv) the assumptions of validity for Eq. (6) reported above.

The model for the cathode is obtained by simplifying the equations of change, taking into account the assumptions listed above, thus yielding:

$$\begin{aligned}
&\frac{\partial \rho_i}{\partial t} + \nu_y \frac{\partial \rho_i}{\partial y} = -\rho_i \frac{\partial \nu_y}{\partial y} + n_e \frac{i}{2FL} M_i \\
&\rho_c \left(\frac{\partial \nu_i}{\partial t} + \nu_y \frac{\partial \nu_y}{\partial y} \right) = -\frac{\partial P_c}{\partial y} \\
&\rho_c \frac{c_{vc}}{M_c} \left(\frac{\partial T_c}{\partial t} + \nu_y \frac{\partial T_c}{\partial y} \right) = \\
&-\frac{\partial}{\partial x} \left(-k_c \frac{\partial T_c}{\partial x} \right) - \frac{\partial}{\partial y} \left(-k_c \frac{\partial T_c}{\partial y} \right) - P_c \frac{\partial \nu_y}{\partial y} + \frac{h_c}{L} (T_E - T_c)
\end{aligned} \tag{8}$$

In which the enthalpy transport between the gas phase and the electrode pores is neglected.

The density of each component, temperature, and velocity are specified on input:

$$\begin{cases}
\bar{\rho}\left(0 \le x \le L_x, y = 0, \forall t\right) = \bar{\rho}^{in} \\
T\left(0 \le x \le L_x, y = 0, \forall t\right) = T^{in} \\
v\left(0 \le x \le L_x, y = 0, \forall t\right) = v^{in}
\end{cases} \tag{9}$$

Having defined (Figure 3) y as the direction of the flux, x perpendicular to y, and z the height of the cell at the entrance, the boundary conditions (BC) for velocity, density, temperature, and heat fluxes at the walls in the x direction are zero. The first and third BC in Eq. (10) are necessary for the momentum ($\rho^* v$), and the second and fourth BC are required for the adiabatic condition. The BC for the heat flux is necessary because, in the present model, heat conduction is not constant and therefore the BC on temperature only is not sufficient. Accordingly:

$$\begin{cases}
\frac{\partial \bar{\rho}}{\partial x}\left(x = 0 \wedge x = L_x, 0 \le y \le L_y, \forall t\right) = 0 \\
\frac{\partial T}{\partial x}\left(x = 0 \wedge x = L_x, 0 \le y \le L_y, \forall t\right) = 0 \\
\frac{\partial v}{\partial x}\left(x = 0 \wedge x = L_x, 0 \le y \le L_y, \forall t\right) = 0 \\
q_x\left(x = 0 \wedge x = L_x, 0 \le y \le L_y, \forall t\right) = 0
\end{cases} \tag{10}$$

Similarly, the situation at the anode can be modelled by the following equations and boundary conditions, where the same assumptions as for Eq. (8), on x, y and z, hold:

$$\begin{aligned}
&\frac{\partial \rho_i}{\partial t} + \nu_x \frac{\partial \rho_i}{\partial x} + \rho_i \frac{\partial \nu_x}{\partial x} = \left(n_e \frac{i}{2FL} + n_{WGS}, \tilde{r}_{WGS} \right) M_i \\
&\rho_a \left(\frac{\partial \nu_x}{\partial t} + \nu_x \frac{\partial \nu_x}{\partial x} \right) = -\frac{\partial P_A}{\partial x} \\
&\rho_A \frac{c_{vA}}{M_A} \left(\frac{\partial T_A}{\partial t} + \nu_x \frac{\partial T_A}{\partial x} \right) = \\
&-\frac{\partial}{\partial y} \left(-k_A \frac{\partial T_A}{\partial y} \right) - \frac{\partial}{\partial x} \left(-k_A \frac{\partial T_A}{\partial x} \right) - P_A \frac{\partial \nu_x}{\partial x} + \frac{h_A}{L} (T_E - T_A)
\end{aligned} \tag{11}$$

$$\begin{cases}
\bar{\rho}\left(x = 0, 0 \le y \le L_y, \forall t\right) = \bar{\rho}^{in} \\
T\left(x = 0, 0 \le y \le L_y, \forall t\right) = T^{in} \\
v\left(x = 0, 0 \le y \le L_y, \forall t\right) = v^{in}
\end{cases} \tag{12}$$

$$\begin{cases}
\frac{\partial \bar{\rho}}{\partial y}\left(0 \le x \le L_x, y = 0 \wedge y = L_y, \forall t\right) = 0 \\
\frac{\partial T}{\partial y}\left(0 \le x \le L_x, y = 0 \wedge y = L_y, \forall t\right) = 0 \\
\frac{\partial v}{\partial y}\left(0 \le x \le L_x, y = 0 \wedge y = L_y, \forall t\right) = 0 \\
q_y\left(0 \le x \le L_x, y = 0 \wedge y = L_y, \forall t\right) = 0
\end{cases} \tag{13}$$

The evolution of the water gas shift reaction, as a function of temperature, and of both reactant and product concentration, is considered at equilibrium:

$$\begin{array}{ccccccc}
CO & + & H_2O & \underset{K_{WGS}}{\longleftrightarrow} & H_2 & + & CO_2 \\
-c_{WGS} & & -c_{WGS} & & +c_{WGS} & & +c_{WGS}
\end{array} \tag{14}$$

The equilibrium condition is:

$$\begin{aligned}
\left(c_{H_2} + c_{WGS}\right)\left(c_{CO_2} + c_{WGS}\right) &= K_{WGS}(T)\left(c_{CO} - c_{WGS}\right)\left(c_{H_2O} - c_{WGS}\right) \\
c_{WGS_{H_2}}\, c_{WGS_{CO_2}} &= K_{WGS}(T) c_{WGS_{CO}}\, c_{WGS_{H_2O}}
\end{aligned} \tag{15}$$

in which a mass continuity equation gives the values for the concentrations of the species, the only unknown being c_{WGS}. Eq. (15) is a quadratic equation, and an internal procedure is used to automatically select the only solution of the equation with physical meaning (concentration greater than zero). The continuity equation at the anode is used to express the rate of WGS reaction once the c_{WGS} is known from the solution of Eq. (15).

$$\tilde{r}_{WGS} = \underbrace{v_x \frac{\partial c_{WGS}}{\partial x} + c_{WGS} \frac{\partial v_x}{\partial x}}_{\text{Instantaneous} \Rightarrow \frac{\partial c_{WGS}}{\partial t} = 0} \tag{16}$$

For electrolyte species, all the velocities in the x and y directions are identically equal to zero:

$$\begin{aligned}
&\rho_E \frac{c_{p_E}}{M_E} \frac{\partial T_E}{\partial t} = -\frac{\partial}{\partial x} \left(-k_E \frac{\partial T_E}{\partial x} \right) - \frac{\partial}{\partial y} \left(-k_E \frac{\partial T_E}{\partial y} \right) \\
&-\Delta H_e \frac{i}{2FL} - \Delta H_{WGS} \tilde{r}_{WGS} - \frac{iV}{L} - \frac{h_C}{L} (T_E - T_C) - \frac{h_A}{L} (T_E - T_A)
\end{aligned} \tag{17}$$

$$\begin{cases}
q_x\left(x = 0 \wedge x = L_x, 0 \le y \le L_y, \forall t\right) = 0 \\
q_y\left(0 \le x \le L_x, y = 0 \wedge y = L_y, \forall t\right) = 0
\end{cases} \tag{18}$$

Physical and chemical properties are calculated from internal models available in the process simulator considered for the implementation, and estimated from *ad hoc* correlation equations reported in the literature [11]:

$$E_0 = 1.2723 - 2.7645 * 10^{-4} T_E$$
$$R_e = 0.348 * 10^2 + 4.8 * 10^{-2} e^{6596/T_E}$$
$$\eta_A = 0 \qquad (19)$$
$$\eta_C = 1.38 * 10^{-1} e^{11400/T_E} P_{O_2}^{-0.67}$$

More details on the derivation of the transient model for the cell are reported in [27].

The total balance between the equations and variables is verified for the overall system, and for each single model, before proceeding with the solution of the system of equations.

2.3 The Steady State MCFC and Process Model

The steady state simulation model is based on the approach of Arato et al. [11], as implemented by some of us in a previous paper [17]. The dynamic model of the fuel cell derived in the previous section has been simplified, and a local steady state model has been derived and interfaced with the process simulator. The local behaviour is described as a simple electrical circuit, series of an ideal voltage, determined by the Nernst equation Eq. (4), and an internal resistance, made up by the sum of the three contributions: i) contact resistance (R_c) between the electrode and current, collector, and electrolyte tile, ii) Ohmic resistance (R_e), and iii) polarization contribution (R_p). The first term is found to be constant, the second term is an exponential function of temperature, and the last one depends on both the temperature and partial pressures of the species involved in the electrochemical reaction Eq. (5). All coefficients of this model are obtained by experimental data fittings [17 and references therein].

The main assumptions considered in the model development are: (i) steady state conditions; (ii) the anodic CO electrochemical reaction neglected due to its very low rate; (iii) non-limiting diffusion in the macro-pores of the electrode and in the gas stream; (iv) current collector as an ideal conductor (constant voltage over the whole surface); (v) adiabatic conditions; (vi) water gas shift reaction considered at equilibrium due its high rate; and (vii) ideal gas. It is important to note that diffusion phenomena occur at high reactant utilization, and heavily reduce the device efficiency. For this reason, they must be avoided by defining the cell working conditions in terms of low gas utilization. So, assumption (iii) is justified.

The model considers local temperature, pressure, and composition changes along the gas path in the ducts, due to reactions, heat transfer, and pressure drop. To find the overall cell behaviour, it is necessary to simultaneously solve four sets of equations, i.e., the mass balance for each gas component, the momentum balance for the cathode and anode gas streams, the energy balance, and local kinetics. These equations may be obtained from the general Eqs. (8)–(18). The boundary conditions are the input gas streams temperature, pressure, and composition, and the assumption of adiabatic conditions. The physical and chemical properties are calculated, from internal models available in the process simulator, or estimated from Eq. (19).

Finite difference and relaxation methods have been employed to numerically solve the system of equations in an in-house developed Fortran90 module.

The electricity production process around the MCFC has been modelled using standard simulation modules. All the necessary pre-treatments, independent of process conditions, were not considered, since they can be included in the input conditions.

The reformer and the catalytic burner (Modular Integrated Reformer – MIR), not available as an Aspenplus™ standard module, have been modelled using other available models, i.e., the reformer side has been modelled by a series of adiabatic equilibrium reactors, the burner side as a series of total combustion reactors, and the heat exchange between the two sides by a series of fixed area heat exchangers among the reactors.

The compressor, turbine, and blower are assumed to work isoentropically at a fixed mechanical efficiency, and the flow rate and/or pressure are fixed at the outlet conditions. The heat exchangers, including the cogeneration heat exchanger, have fixed outlet temperatures. Heat losses and pressure drop (except those in the fuel cell) have been neglected.

3 Results and Discussion

Firstly, the simulation results are presented for the entire electricity production process, in which the simplified model of the MCFC is used at steady state, with the aim of determining the behaviour of the process. Subsequently, the steady state and dynamic behaviour of the MCFC are reported in order to understand the detailed behaviour of the cell in terms of sensitivity of a set a variables and the open loop response during transients.

3.1 Steady State Analysis of the Process

The process simulations reported in this work were performed by Aspen plus™. Default Aspen plus™ models have been used for traditional plant units, while for fuel cell stack the custom Fortran90 code described above was used and integrated in the simulation flow sheet.

Fuel cell efficiency is defined as the ratio of the electrical power produced by the stack and the chemical power of the fuel actually consumed. Referring the efficiency to total fuel energy input could be misleading because residual fuel is doubly recovered. In the catalytic burner, part of the heat produced is transferred to the reformer, where it is converted to chemical energy by means of endothermic reactions. In addition, another part of the gas energy is recovered in the turbine. This recovery of energy takes place with less efficiency than fuel cell conversion. Hence, to achieve high system efficiency, it is useful to assign the highest possible energy to

electrochemical conversion. The process (Figure 1) can be considered as a fuel cell/gas turbine hybrid cycle (FC/GT), where the topping cycle is the FC and the bottoming one is the GT. It is useful to consider the variables that affect the bottoming cycle behaviour. For a gas turbine system, the efficiency is improved by a high pressure ratio and high turbine input gas temperature. In the present case, the FC and Modular Integrated Reformer (MIR) [17] substitute for the combustion chamber, but the qualitative trend remains unchanged.

To assure consistency between the process model and the detailed simulation of the MCFC, thus obtaining the practical advantages listed in the introduction in terms of temperature and concentration distributions, it is necessary to set up the process simulation with particular care to avoid numerical instabilities and unrealistic conditions both in the process and in the MCFC. In particular, great attention has been paid to (i) the initialisation of the variables at each run, (ii) the convergence of the recycles and the tearing streams, (iii) the verification of the MCFC input conditions, and (iv) the sensitivity analysis.

Simulations start with a "base case" in which all the assumptions are used as preliminary project specifications. Base case input specifications and simulation results are reported in Table 1. Base case results report a relatively low overall process electrical efficiency. In order to obtain a higher efficiency, a modification of the base case was conducted to account for the combustion of all the residual fuel before the heat exchange with the gas to be reformed. The results of the modified base case are reported in Table 1 (column 4), and the numerical values are shown in Figure 1. These results agree with expectations for similar systems [29] and seem to predict a better performance with respect to experimental results for ambient pressure systems without GT integration [30]. Process parameters were varied in the sensitivity analysis, and the relevant results are briefly summarized in Table 2. Sensitivity analysis of the process shows that an increase in the steam to methane ratio (the main parameters of the process) results in an improvement in the reforming and gas shift equilibrium, as the amount of one of the reactants is increased. In spite of a slight reduction in fuel cell efficiency, due to reactant dilution, the overall electrical efficiency improves. Two main reasons can be invoked to account for this behaviour: (i) more energy is converted in the FC stack where the efficiency is higher since a higher amount of hydrogen available, and (ii) more heat is removed by the anode exhaust gas, and so more heat is recycled into the plant and in the bottoming cycle, increasing its efficiency. Pressure has different effects on electrical efficiency in different parts of the plant. The effect of an increase in pressure shows that the increase of the two cycle efficiencies overcomes the decrease of methane conversion effect. Nevertheless, there is a worsening of cogeneration, because residual heat again exits in a more degenerated form. The fresh air flow rate does not affect the cells, bottoming cycle, and cogenerative efficiencies, but shows a reduction in system electrical efficiency as the air flow rate is increased [17].

Table 2 Sensitivity analysis for a variation of steam to methane ratio, air flow rate, and pressure.

	Steam to methane ratio / H_2O/CH_4			
	3	4	4.5	5.5
Electrical plant efficiency /%	54.8	56.3	57.1	57.7
Stack efficiency /%	59.7	58.8	58.3	57.5
Cell voltage / V	0.761	0.748	0.741	0.730
CH_4 conversion /%	88.7	92.3	94	96.6
Bottoming cycle efficiency /%	13.2	14.3	14.8	16.2
Cogenerative efficiency /%	75.6	71.8	69.8	65.8
	Air flow rate / kg h^{-1}			
	1980	2050	2250	
Recirculation /%	55.7	57	60	
Reforming temperature / C	742	740	727	
CH_4 conversion /%	91.4	91.1	88.7	
	Pressure / bar			
	3	3.5	4	5
Electrical plant efficiency /%	53.8	54.6	55.3	56.3

3.2 Steady State Simulation of the MCFC

The dynamic model of the MCFC, briefly described above, was implemented in the Aspen Custom Modeler™ (ACM). The ACM allows both steady state and dynamic simulations to be carried out using the same set of equations. In general, the numerical solution of the system of partial differential equations was carried out by the method of lines. A variable step implicit Euler method was selected, among other methods tested, for its efficiency and accuracy. A Fast Newton method was used as a non-linear solver.

The model input variables are scalar properties (velocity, temperature, and density of each species, average cell current), the state (internal) variables are distributed variables in the region of the simulation (velocity, temperature, density, pressure, thermo physical properties,...), while the output variables are the same as the input plus the electrical variables (voltage, current and power) and the mean state variables.

With the model set up and tested, steady state simulations were run in ACM for at least three fundamental reasons: (i) to compare data and profiles

Table 1 Input specifications and base case results of steady state simulation of the MCFC.

Input specifications		Process variables	Base case	Modified Base case
Cell solid temperature / °C	650	CH_4 plant feed rate / kg h^{-1}	82.0	74.5
Fuel utilisation /%	75	Stack power / kW	505.6	502.1
Oxygen utilisation /%	30	Bottoming cycle power / kW	77.5	66.2
Pressure / bar	3.5	Thermal cogeneration power / kW	261	215
Steam/methane ratio	3	Reforming temperature / °C	688	727
Steam temperature / °C	170	CH_4 conversion /%	79.3	88.7
		Stack efficiency /%	60.3	59.7
		Cell voltage / V	0.769	0.761
		Bottoming cycle efficiency /%	12.2	12.4
		Overall process electrical efficiency /%	51.1	54.8
		Cogenerative efficiency /%	74.0	75.6

obtained with literature results, (ii) to get starting points for dynamic simulations, and (iii) to estimate the capability of the model to follow the evolution of variables with time from a steady state to the case after a perturbation.

Steady state simulation started from the "base case" in which convergence was achieved for all the variables at a steady state and for the input conditions corresponding to those available in the literature [9, 17, 28]. Results are reported in Table 1. The base case results were obtained by adjusting the numerical values of the parameters included in the relationship expressing Nusselt as a function of Reynolds and Prandtl to get temperature profiles close to the literature values [17].

The validation of the base case was done by comparing the simulated data with literature experimental evidence: [9] reports a mean temperature of 932 K (for a system very similar to the one reported in this work) and [16] reports a hot spot of 983 K in the same position predicted by the model developed in this work. References [9, 10, 18], from which experimental correlations were taken, also show good agreement in variable distributions and three-dimensional diagrams. Steady state results for the base case and for all the steady state conditions investigated are summarized in Table 3a and b.

Table 3a Dynamic model under steady state conditions: input and output variables for base case and sensitivity analysis. Input variables modified for each analysis are reported, velocity (v), temperature (T), pressure (P), current density (i), keeping the other values fixed at the base case.

	Base case	v (1, 6)	T (840, 830)	P (2.5, 3.5)	i (1.7)	
Input variables						
$v\|_{(x\ 0)}$	1.188	1.000				m h^{-1}
$v\|_{(0\ y)}$	5.479	6.000				m h^{-1}
$T\|_{(x\ 0)}$	870.000		840.000			K
$T\|_{(0\ y)}$	860.000		830.000			K
$P\|_{(x\ 0)}$	3.500		3.380	2.500		bar
$P\|_{(0\ y)}$	3.500		3.378	3.500		bar
$\langle i \rangle$	1.500				1.700	kA m^{-2}
Output variables						
U_{H_2}	75.000	82.279	75.132	89.450	80.746	%
U_{O_2}	30.000	28.041	30.955	30.812	34.780	%
T_A^{out}	930.291	930.213	909.522	936.135	946.345	K
T_C^{out}	952.924	954.152	932.395	963.654	974.373	K
$\langle T_E \rangle$	938.940	940.768	919.678	948.464	957.827	K
i_0^0	0.024	0.025	0.015	0.029	0.027	kA m^{-2}
$\langle V \rangle$	1.092	1.081	1.069	1.083	1.076	V
$\langle W \rangle$	1.636	1.620	1.599	1.625	1.827	kW m^{-2}

Table 3b cont...

	Base case	v (1, 6)	T (840, 830)	P (2.5, 3.5)	i (1.7)	
Input variables						
$\rho_{CH_4}^{in}$	5.00E-05					kg m^{-3}
ρ_{CO}^{in}	1.10E-01			7.85E-02		kg m^{-3}
$\rho_{CO_{2_A}}^{in}$	1.51E-01			1.08E-01		kg m^{-3}
$\rho_{H_2}^{in}$	7.91E-02			5.65E-02		kg m^{-3}
$\rho_{H_2O}^{in}$	4.42E-02			3.15E-02		kg m^{-3}
$\rho_{CO_{2_C}}^{in}$	5.89E-01					kg m^{-3}
$\rho_{N_2}^{in}$	8.06E-01					kg m^{-3}
$\rho_{O_2}^{in}$	2.38E-01					kg m^{-3}
Output variable						
$\rho_{CH_4}^{out}$	3.17E-05			2.79E-05		kg m^{-3}
ρ_{CO}^{out}	7.43E-02	6.09E-02	7.21E-02	3.28E-02	6.55E-02	kg m^{-3}
$\rho_{CO_{2_A}}^{out}$	7.41E-01	8.29E-01	7.33E-01	6.51E-01	7.87E-01	kg m^{-3}
$\rho_{H_2}^{out}$	1.98E-02	1.40E-02	1.97E-02	5.96E-03	1.52E-02	kg m^{-3}
$\rho_{H_2O}^{out}$	3.17E-05			2.79E-05		kg m^{-3}
$\rho_{CO_{2_C}}^{out}$	3.88E-01	4.02E-01	3.83E-01	3.84E-01	3.57E-01	kg m^{-3}
$\rho_{N_2}^{out}$	8.61E-01	8.46E-01	8.49E-01	8.51E-01	8.63E-01	kg m^{-3}
$\rho_{O_2}^{out}$	1.67E-01	1.71E-01	1.64E-01	1.65E-01	1.55E-01	kg m^{-3}

The velocities reported in Table 3 refer to single cell velocities required to reach the desired hydrogen utilization, their numerical value is consistent with literature values of around 1 mol h^{-1} [7, 12, 13]. Output temperatures and mean electrolyte temperatures are rather high and close to the highest acceptable values. A sensitivity analysis at steady state (Table 3) is carried out to understand how changes in the given process variables affect process conditions. In this work attention was focused on the input temperatures, velocities, mean current density, and pressure. Table 3 shows all the results of the cell sensitivity analysis. Column 3 in Table 3 shows the inverse relationship between inlet velocity and utilization at both electrodes, column 4 shows the effect of temperature, which is not proportional to the generating cause, column 5 shows that a decrease of the anode pressure gives a very small U_{H2}. Finally, column 6 reports that an increase in the current density of about 13% results in a temperature outside the acceptable operating range for a MCFC.

3.3 Dynamic Simulation of the MCFC

The model is tested under transient conditions by changing one or more of the input variables, one at a time or simultaneously, with different kinds of perturbations at one or both of the electrodes. The starting condition was always assumed to be the steady state condition of the base case. In order to

check that a reliable steady state is always reached after the transient time, deviations between the dynamic values and the new steady state values are checked after 60 h of simulated time. The deviations are always less than 0.1% for the cases reported in Table 3.

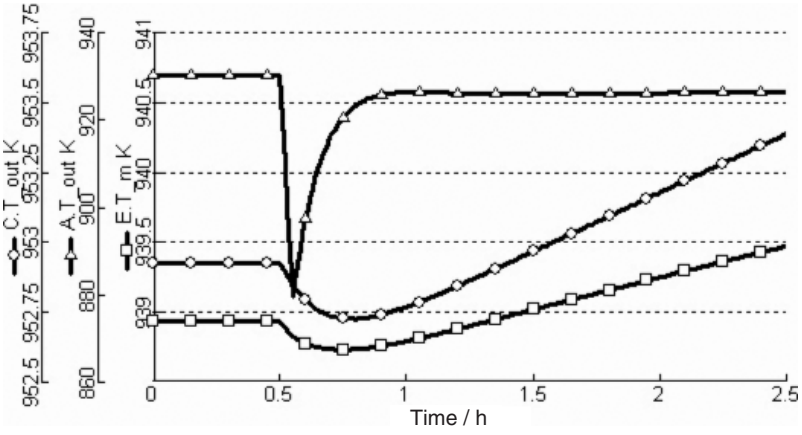

Fig. 4 Temperature profiles as a function of time, after a 1 bar step, reducing anode pressure.

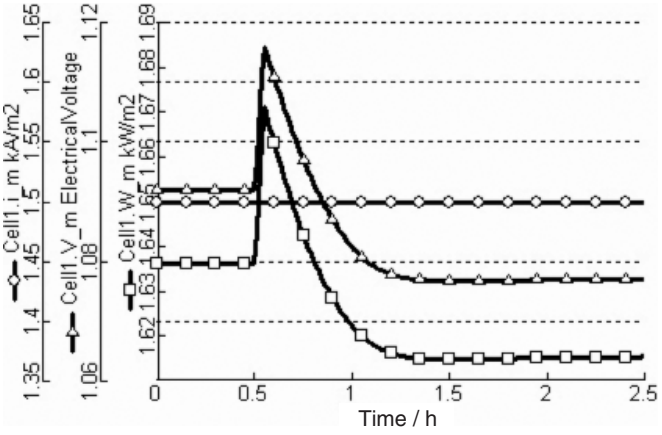

Fig. 5 Electrical property profiles as a function of time, after a 1 bar step, reducing anode pressure.

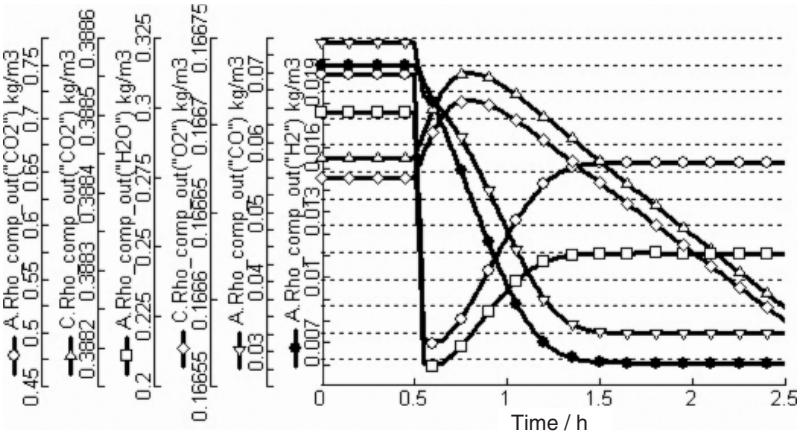

Fig. 6 Density profiles as a function of time, after a 1 bar step, reducing anode pressure.

3.3.1 *Pressure Perturbation*

Pressure perturbation in one part of the cell is one of the transient behaviours relevant for industrial applications, since it may be due to a pumping system failure. In the following analysis open loop behaviour (i.e. no control action) is assumed, since our purpose is to illustrate the model behaviour. A pressure reduction of 1 bar at the inlet stream of the anodic compartment (from 3.5–2.5 bar) is supposed to take place suddenly at time 0.5 h. This variation is obtained by modifying component densities, while keeping the mole fractions constant. Initially, the anode temperature drops rapidly, because of the direct effect (P is proportional to T), and afterwards increases because of the heat of reaction. The rate by which temperature decreases is greater than that by which it increases. Approximately 30 min after the perturbation, the final temperature value is stable at a lower value, according to the steady state analysis. This behaviour spreads, by conduction, to the electrolyte and to the cathode, resulting in a typical inverse response (Figure 4).

At the beginning, the potential increases as V is proportional to $\ln(P_A^{-1})$ and therefore to P_A^{-1}. This is a consequence of the constant pressure at the cathode, and the constant molar fraction at the anode, which overall results in the inverse relationship between V and P. After this initial behaviour, the decrease in E_0 with increasing temperature dominates (Figure 5), and accordingly, V decreases. The reaction rate is a function of the current, which in turn is a function of temperature; this effect is included in the model.

In Figure 6, the density profiles are reported as a function of time for all the species of interest. The profiles reported are a consequence of the attainment of new equilibrium conditions in the WGS reaction.

The response to a perturbation can also be studied for the distributed variables on the cell plane. In this case, the presence of an anode temperature hot spot can be noted at steady state, in the furthermost corner from the input sections. This is due to the progressive heating of the relatively cold gases at both electrodes (Figure 7). The evolution, with time, of the temperature profiles and hydrogen concentration profiles is available in AVI format [31].

3.3.2 *Velocity Perturbation*

The anode and cathode velocities have been perturbed. The velocity has been reduced (v_A = 1.0 m h^{-1}) at the anode and increased (v_C = 6.0 m h^{-1}) at the cathode to obtain a

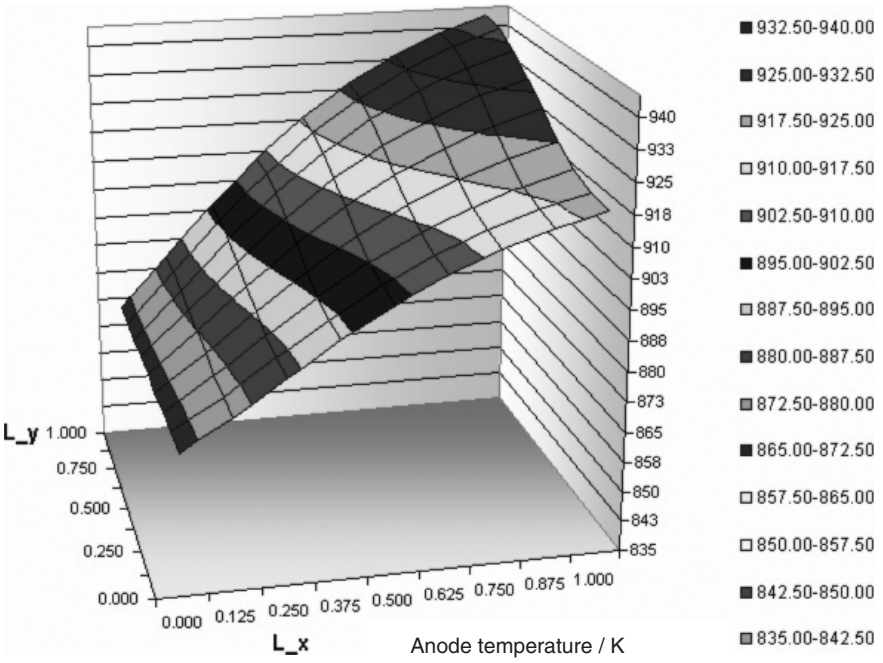

Fig. 7 Anode temperature distribution on the cell plane at steady state.

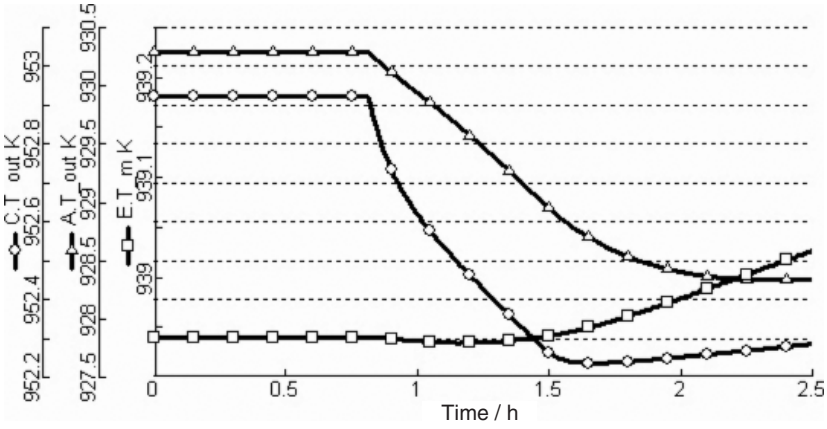

Fig. 8 Temperature profiles as a function of time, after two diverging linear ramps in electrode velocities (decreasing at anode and increasing at cathode).

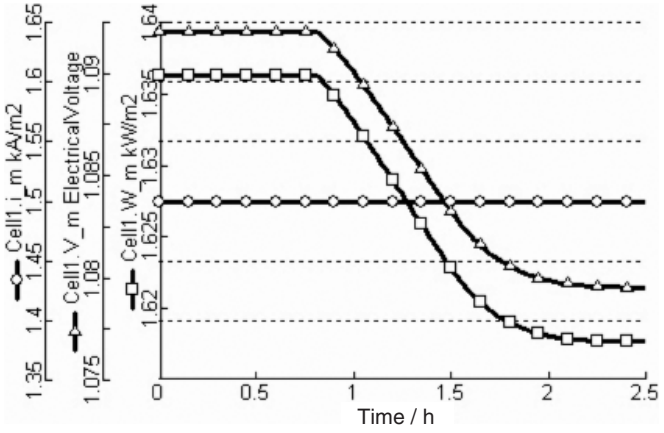

Fig. 9 Electrical property profiles as a function of time, after two diverging linear ramps in electrode velocities (decreasing at anode and increasing at cathode).

reduced hydrogen output for bottoming operations and less oxygen utilization. The perturbations are applied at the same time for 0.5 h, with a linear ramp for 1.0 h.

Figures 8–10 report time evolution after two diverging linear ramps in electrode velocities for the variables of interest, namely temperature (Figure 8), electrical properties (Figure 9), and densities (Figure 10). The distribution of voltage on the cell plane shows a progressive lowering, concentrated near the output section of the anode, and a stronger dependence on anode rather than cathode partial pressures. The evolution of the voltage distribution profiles on the cell plane, with time, is available in AVI format [31].

3.3.3 *Temperature Perturbation*

Both the anode and cathode temperatures are supposed to vary smoothly, with a semi-sinusoidal shape, with the same intensity (30 K less than the base case, corresponding to T_A = 840 K and T_C = 830 K) but at different times (0.5 h and 0.75 h, respectively) and for different durations (1.0 h and 0.5 h, respectively).

The mean anode temperature at the output section reacts to a semi-sinusoidal input with a semi-sinusoidal response; the cathode response tends to be sinusoidal in behaviour, but it is smoothed by the time delay. Figures 11–13 report time evolution after two sinusoidal ramps in electrode temperatures for the variables of interest, namely temperature (Figure 11), electrical properties (Figure 12), and densities (Figure 13).

3.3.4 *Current Perturbation*

Modern molten carbonate fuel cells work at 1.5 kA m^{-2}. The model investigates the effect of a larger current density (of 1.7 kA m^{-2}) assuming a step at time 0.5 h. As expected, the voltage decreases as the polarization increases with current.

Figures 14–16 report the time evolution after a step in current density for the variables of interest, i.e., temperature (Figure 14), electrical properties (Figure 15), and densities (Figure 16). The anode temperature (Figure 14) initially decreases,

due to the WGS, which reaches a new equilibrium with the production of H_2 consuming heat (endothermic reaction), and finally increases, due to the heat of reaction of the electrochemical reaction.

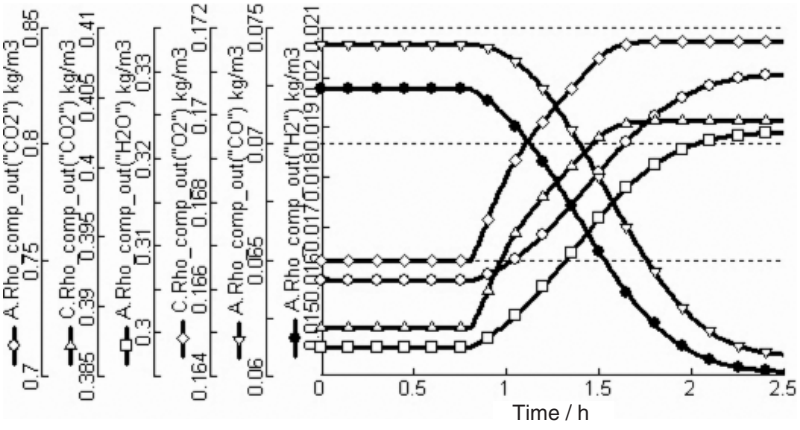

Fig. 10 Density profiles as a function of time, after two diverging linear ramps in electrode velocities (decreasing at anode and increasing at cathode).

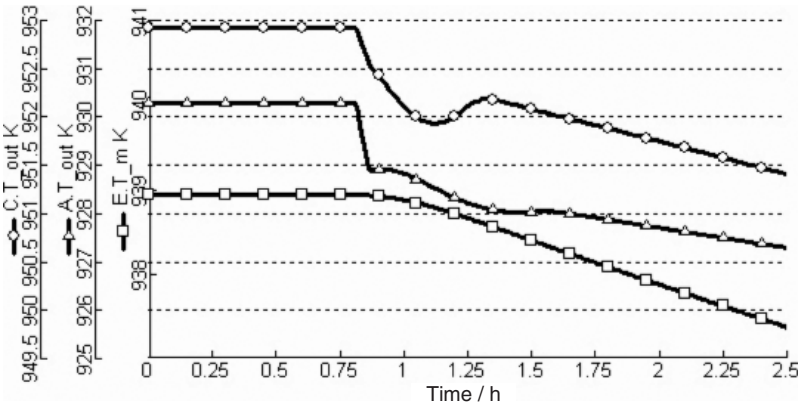

Fig. 11 Temperature profiles as a function of time, after two semi-sinusoidal decreasing ramps in electrode temperatures.

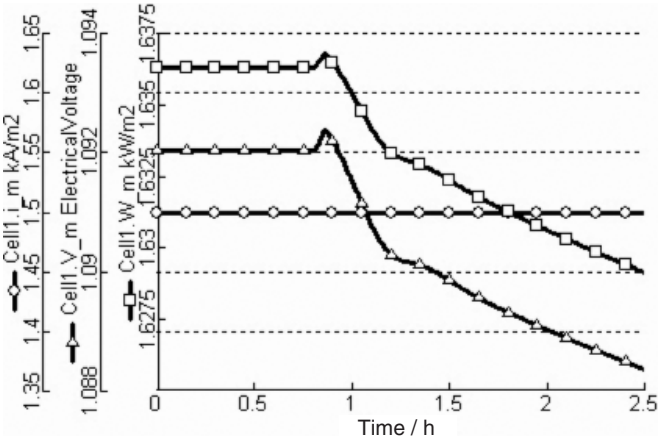

Fig. 12 Electrical property profiles as a function of time, after two semi-sinusoidal decreasing ramps in electrode temperatures.

4 Conclusions

This paper has presented the results of a steady state simulation of the electricity production process based on a MCFC coupled with a consistent detailed steady state and dynamic simulation of the single cell. Both the process and cell models have been briefly presented and discussed, referring to the literature for the implementation details. Base cases and sensitivity analysis have been reported for both the process and the cell. The cell has been studied in steady state and dynamic conditions, thus evidencing key parameters for the behaviour of the system.

The steady state simulation of the MCFC system has enabled a deep understanding of the electrochemical behaviour of the device, useful for its integration with other units. Calculations showed that overall electrical efficiency can easily be kept above 50–55%, derived from about 60% for the fuel cell stack and 12% for the bottoming cycle. Cogenerative efficiency in the simulation remains at about 75%. The simulation showed that if the anode exhaust gas is burned before heat exchange with the reformer, a higher conversion is obtained and the overall electrical and cogenerative efficiencies rise from 51.1 and 74 to 54.8 and 75.6%, respectively. These results agree with expectations for similar systems [29] and predict better performance with respect to results for an ambient pressure system without GT integration [30]. The process sensitivity analysis showed that there is still room for improvement in electrical efficiency by increasing the steam to methane ratio, the pressure, and decreasing the air feed rate, but keeping in mind that all these variables will inevitably worsen the cogeneration.

The detailed steady state simulation of the MCFC showed the inverse relationship between inlet velocity and utilization at electrodes, the effect of process variables on temperature distribution, and the effect of anode pressure.

From the dynamic simulation results for the MCFC, it can be concluded that the behaviour of the molten carbonate fuel cell, within an acceptable operating range of variables, is strongly influenced by the input temperature and even more so by utilization and the mean current density desired. The simulation showed that under certain conditions, high temperature distributions and peaks are present in the cell as well as the possible occurrence of the inverse behaviour of some state variables.

In summary, the paper reports the results of a process simulation for a realistic configuration of an electricity production system by a MCFC

able to focus on the macroscopic quantities of interest such as stack efficiency, system process electrical efficiency, and cogenerative efficiency. In addition, this was integrated with a consistent dynamic model of the cell, which was able to consider the behaviour of microscopic and distributed variables such as temperature and concentration.

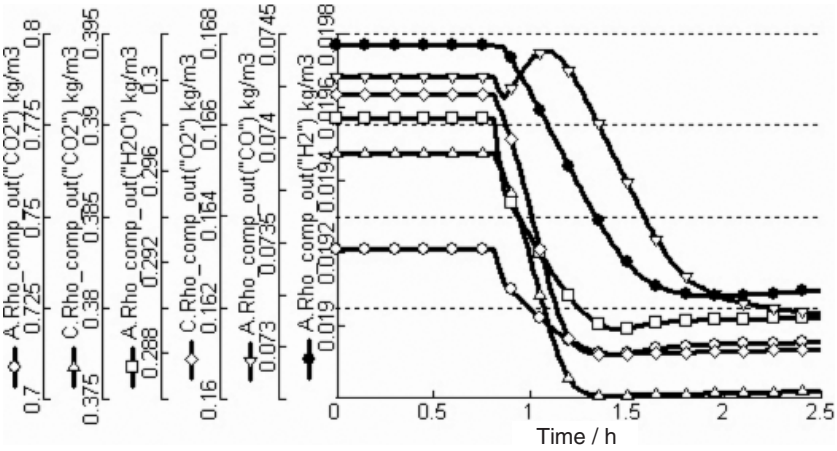

Fig. 13 Density profiles as a function of time, after two semi-sinusoidal decreasing ramps in electrode temperatures.

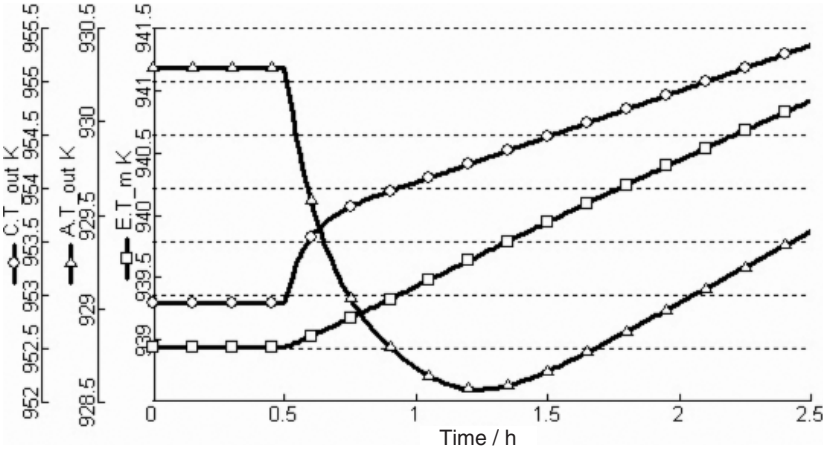

Fig. 14 Temperature profiles as a function of time, after a 0.2 kA m^{-2} step increase in current density.

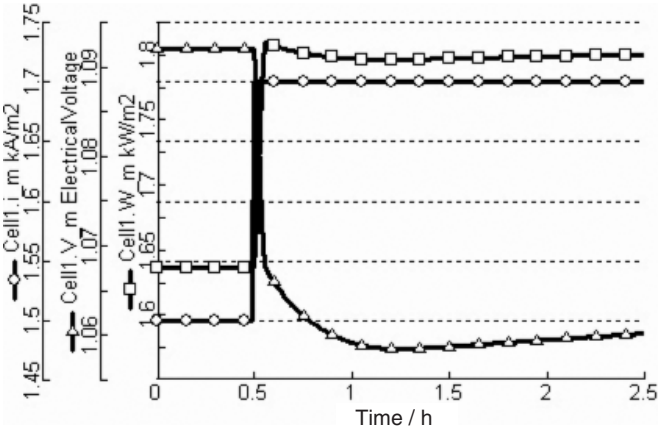

Fig. 15 Electrical property profiles as a function of time, after a 0.2 kA m^{-2} step increase in current density.

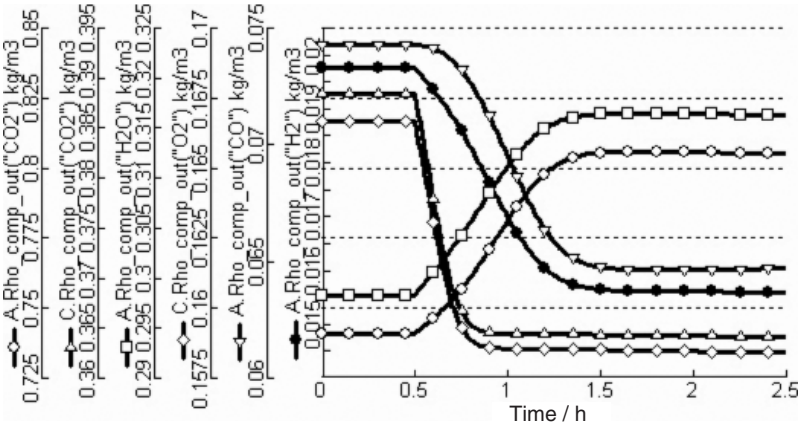

Fig. 16 Density profiles as a function of time, after a 0.2 kA m^{-2} step increase in current density.

Acknowledgments

The authors wish to thank F. Parodi (Ansaldo Fuel Cells S.p.a) and R. Taccani (University of Trieste) for helpful discussions.

List of Symbols

Latin letters

A	Anode
c	Specific heat, Concentration/ kJ $kmol^{-1}$ K^{-1}, mol m^3
C	Cathode
E	Standard Equilibrium potential /V
F	Faraday's constant / kC mol^{-1}
h	Heat transfer coefficient / W m^{-2} K^{-1}
i	Current density / kA m^{-2}
L	Length / m
k	Thermal conductivity / W m^{-1} K^{-1}
K	Equilibrium constant
M	Molar weight / kg $kmol^{-1}$
n	Number of moles
P	Pressure / bar
q	Energy flux / W m^{-2}
r	Reaction rate / mol m^{-3} h^{-1}
R	Gas constant, Resistance / J mol^{-1} K^{-1}, Ω mm^2
t	Time / h
T	Temperature / K
U	Utilization
v	Velocity / m h^{-1}
V	Voltage / V
W	Power / W
WGS	Water Gas Shift
x	Molar fraction
x, *y*	Coordinates / m

Greek letters

β	Symmetry factor
Δ	Variation
ρ	Density / kg m^{-3}
η	Polarization / Ω mm^2

Super scripts

0	Standard
+, –	Ionic charge
eq	Equilibrium
in	Inlet
out	Outlet
r	Reaction

Sub scripts

0	Open circuit / Exchange / Standard
e	Electrical
E	Electrolyte
I	Generic component
p	Constant pressure
r	Mass generation / Reaction
v	Velocity / Constant volume
x, *y*	Coordinates

Over signs

→, ←	Reaction direction
__	Vector / Tensor
~	Molar based
^	Mass based

References

[1] G. J. Kraaij, G. Rietveld, R. C. Makkus, J. P. P. Huijsmans, *J. Power Sources* **1998**, *71*, 215.
[2] M. Bishoff, G. Huppman, *J. Power Sources* **2002**, *105*, 216.
[3] K. Joon, *J. Power Sources* **1996**, *61*, 129.
[4] A. B. Hart, G. J. Womack, *Fuel cells, theory and application*, Chapman and Hall LTD, London, **1967**.
[5] K. Kordesh, G. Simander, *Fuel cells and their applications*, VCH, Weinheim, **1996**.
[6] B. S. Kang, J.-H. Koh, H. C. Lim, *J. Power Sources* **2001**, *94*, 51.
[7] Y. Miyake, N. Nakanishi, T. Nakajima, Y. Ytoh, T. Saitoh, A. Saiai, H. Yanaru, *J. Power Sources* **1995**, *56*, 11.
[8] F. Yoshiba, N. Ono, Y. Izaky, T. Watanabe, T. Abe, *J. Power Sources* **1998**, *71*, 328.
[9] B. Bosio, P. Costamagna, F. Parodi, *Chemical Engineering Science* **1999**, *54*, 2907.
[10] J.-H. Koh, B. S. Kang, H. C. Lim, *J. Power Sources* **2000**, *91*, 161.
[11] E. Arato, B. Bosio, P. Costa, F. Parodi, *J. Power Sources* **2001**, *102*, 74.
[12] M.-H. Kim, H.-K. Park, G.-Y. Chung, H.-C. Lim, S.-W. Nam, T.-H. Lim, S.-A. Hong, *J. Power Sources* **2002**, *103*, 245.
[13] H.-K. Park, Y.-R. Lee, M.-H. Kim, G.-Y. Chung, S.-W. Nam, S.-A. Hong, T.-H. Lim, H.-C. Lim, *J. Power Sources* **2002**, *104*, 140.
[14] M. Mangold, M. Sheng, *AIChE's Annual Meeting*, **2003**, p. 169a.
[15] J.-H. Koh, B. S. Kang, H. C. Lim, *A.I.Ch.E. Journal* **2001**, *47*, 1941.
[16] W. He, Q. Chen, *J. Power Sources* **1995**, *55*, 25.
[17] G. De Simon, F. Parodi, M. Fermeglia, R. Taccani, *J. Power Sources* **2003**, *115*, 210.
[18] E. Fontes, M. Fontes, D. Siminsson, *Electrochimica acta* **1995**, *40*, 1641.
[19] E. Fontes, C. Lagergren, D. Siminsson, *J. of Electroanalytical Chemistry* **1997**, *432*, 121.
[20] J. D. Fehribach, J. J. A. Prins, K. Hemmes, J. H. W. De Wit, F. W. Call, *J. of Applied Electrochemistry* **2000**, *30*, 1015.
[21] T. Shinoki, M. Matsumura, A. Sasaki, *IEEE Transaction on Energy Conversion* **1995**, *10*, 722.
[22] W. He, *International Journal of Energy Research* **1997**, *21*, 69.
[23] W. He, *Energy Conversion and Management* **1998**, *39*, 775.
[24] M. D. Lukas, K. Y. Lee, A. H. Ghezel, *IEEE Transaction on Energy Conversion* **2001**, *16*, 289.
[25] P. Heidebrecht, K. Sundmacher, *Chemical Engineering Science* **2003**, *58*, 1029.
[26] G. De Simon, *Thesis*, University of Trieste, Italy, **2002**.
[27] A. Cudicio, *Thesis*, University of Trieste, Italy, **2003**.
[28] B. Bosio, P. Costamagna, F. Parodi, B. Passalacqua, *J. Power Sources* **1998**, *74*, 175.
[29] R. A. George, *J. Power Sources* **2000**, *86*, 134.
[30] M. Gnann, *Abstracts of the VII Grove Fuel Cell Symposium*, London, **2001**, p. 58.
[31] WWW.CASLAB.UNITS.IT.